Journal of the Brazilian Society of Mechanical Sciences and Engineering (2018) 40:442
https://doi.org/10.1007/s40430-018-1365-4

TECHNICAL PAPER

Mechanical design and preliminary tests of VS-AnkleExo

Ozgur Baser[1] · Hasbi Kizilhan[1]

Received: 9 January 2018 / Accepted: 14 August 2018 / Published online: 23 August 2018

Abstract
Exoskeletons and wearable robotic systems have advanced substantially over the last decade for gait assistance, rehabilitation and load-carrying purposes. Currently, there are commercially available devices with stiff actuators. However, these actuators cannot adapt to their unpredictable environments. Thus, compliant actuators like series elastic and variable stiffness actuators have been implemented in exoskeletons and active orthoses. This paper presents a novel design and experimental characterization of a compliant actuator with adjustable stiffness for a lower limb wearable ankle robot (VS-AnkleExo). The proposed actuator is designed to mimic the behavior of biological ankle and maximizes the compliance between user and robot during a gait cycle. The adjustable stiffness of actuator is achieved through a controllable transmission ratio mechanism. Both transparency and tracking performance experiments are performed to demonstrate reduced the user–robot interaction force and improved the tracking performance of the proposed actuator, respectively. Experimental results showed that interaction forces between the user and robot are minimized in the transparency experiments, while the actuators proposed are able to track the given torque signals at various frequencies in the tracking experiments.

Keywords Ankle exoskeleton · Variable stiffness actuator · Controllable transmission ratio actuator · Force/torque control · Transparency

1 Introduction

Exoskeleton robots are a special class of devices where the robot works cooperatively with human. These types of devices act as a second skeleton to support the human motion to achieve certain tasks. Hence, they have been used in various applications including stroke rehabilitation, motion assist for handicapped people and military applications [1–3]. The exoskeleton robots that are used for rehabilitation and motion assist generally require special attention in terms of structural components to ensure the safety and adaptability of the device. Hence, high precision actuators are replaced with structurally compliant actuators for these kinds of devices [4]. The compliance of the actuators can be directly obtained by using passive elements such as springs. One of the examples of a compliant actuator with a passive element is series elastic actuator [5]. In the literature, various compliant actuators exploiting the advantages of passive elastic elements to regulate output stiffness have been proposed. Kizilhan et al. divided these actuators into 5 different categories [6]: (1) equilibrium-controlled stiffness [5], (2) antagonistic-controlled stiffness [7–11], (3) structurally controlled stiffness [12], (4) mechanically controlled stiffness [13, 14] and (5) controllable transmission ratio stiffness [15–17]. Compliant actuators have been used in various exoskeletons because of their ability to absorb forces and store/release power during their use. The devices with compliant actuators such as serial elastic actuators include: RoboKnee [18], IHMC [19] and LOPES [20, 21]. Even though the serial elastic actuators have several advantages over the other types of actuators, their compliance cannot be changed. However, the robot joint stiffness should be adjusted such that the robot can handle the environmental changes experienced by the user. Hence, different exoskeleton designs using variable stiffness actuator have been proposed, especially for motion assist and

Technical Editor: Victor Juliano De Negri.

✉ Ozgur Baser
ozgurbaser@sdu.edu.tr

Hasbi Kizilhan
hasbikizilhan@sdu.edu.tr

[1] Department of Mechanical Engineering, Suleyman Demirel University, Isparta, Turkey

rehabilitation. The exoskeletons using these actuators include: ALCATRO [22], KNEXO [23] and ATLAS [24].

To obtain accurate and stable interactions with humans, the exoskeletons using compliant actuators involve force (or torque) mode control. In the last decade, cascade control structures have drawn significant attention for series elastic actuators [25]. In this structure, nested control loops have been adopted to ensure the stability of the system. To control the dynamic response of the serial elastic actuators, an inner loop controlling the force/torque response has been adopted and coupled with an outer loop impedance controller to carry out high-level control tasks [20, 26]. Moreover, a velocity loop has been incorporated in various studies into the torque loop to use the motors as a velocity source in the system [27–29].

Impedance control is another desirable control method to ensure an accurate and stable control between the exoskeleton and user. The impedance controller controls the interaction forces between exoskeleton and user. In this control scheme, the output of the impedance controller becomes the reference force for force/torque controller. Thus, the force/torque of the exoskeleton is close or equal to the reference force input. The main goal is to provide aid to the users in performing tasks such that the exoskeleton–user interaction forces become zero. This control method allows high impedance during the robot-in-charge mode to bring the robot to a specific position, while it can remove the forces exerted by the system to the user when it is in human-in-charge mode [30].

In this research, the performance of the impedance control method has been investigated on VS-AnkleExo which can adjust its stiffness. First, the exoskeleton actuator design is briefly explained and compared to the available designs in the literature by simulating the power consumption. Then, an impedance control diagram is developed and used to control the actuator located on VS-AnkleExo. The performance of the device and the controller has also been evaluated in two different modes: (1) human-in-charge and (2) robot-in-charge. In the following sections, the biomechanics of a human ankle joint is briefly introduced and followed by the comparison of the existing actuator designs in the literature. Then, the details of VS-AnkleExo and the developed impedance control scheme are presented. This is followed by the experimental results and their discussion on the performance of the device developed in terms of transparency and the tracking performance.

2 Development of compliant actuator

2.1 The biomechanics of human ankle joint

Understanding the basics of human motion is important to develop exoskeleton robots since the joints' position, velocity, acceleration and torque change significantly during a gait cycle. Hence, the phases of ankle motion and stiffness changes during a gait cycle should be identified for an ankle exoskeleton robot. The ankle undergoes stance and swing phases during one gait cycle. It presents an initial plantar-flexion at the first 10% of gait cycle until the foot lies on the ground [31]. Then, the motion of the ankle depends on the progression of the body. The progression period is divided into different sub-phases and includes: (1) dorsi-flexion (Fig. 1b–c), (2) dual-flexion (Fig. 1c–d) and (3) plantar-flexion (Fig. 1d–e). (Figure 1a–b can be neglected because the ankle exhibits only plantar-flexion motion) [31]. The ankle shows a relatively slow motion during the swing phase. Hence, the current research only focuses on the progression period because the ankle exhibits the highest movement during this phase of the walking. Moreover, the quasi-stiffness of the ankle is generally characterized for sub-phases of the stance phase during the progression period. Figure 1 shows the ankle's moment–angle relative curve for a representative subject walking. Dorsi-flexion, dual-flexion and plantar-flexion sub-phases are represented by separate line fitting on the moment–angle curve as shown in Fig. 1. This shows that the ankle neuromuscular system can adjust ankle joint stiffness to different stiffness values for different sub-phases.

2.2 Variable stiffness actuator designs

The actuators used in regular robot applications are preferred to be as stiff as possible to obtain precise movements or to make the trajectory tracking control easy [32]. However, the actuators used in rehabilitation robotics and walking robots are required to be as soft as possible to provide safe human–robot interactions. Hence, it is necessary to use compliant actuators in the robot-human interaction applications.

The compliant actuators can minimize the forces due to shocks, provide safe human–robot interactions and store/release energy with passive elastic elements [32]. Hence, several actuators designs that can vary their stiffness have been proposed in the literature. In this section, we present a novel variable stiffness actuator developed for an ankle exoskeleton robot and its kineto-static analysis. Moreover, the kineto-static analyses of the antagonistic-controlled actuators along with the mechanically controlled actuator are presented and compared to the novel actuator design presented in this research. The details of the kineto-static analyses of the available designs in the literature are given in a previous study [6].

2.2.1 The antagonistic-controlled actuator design

In this design, two series elastic actuators (SEA) with non-adaptable compliance and nonlinear displacement

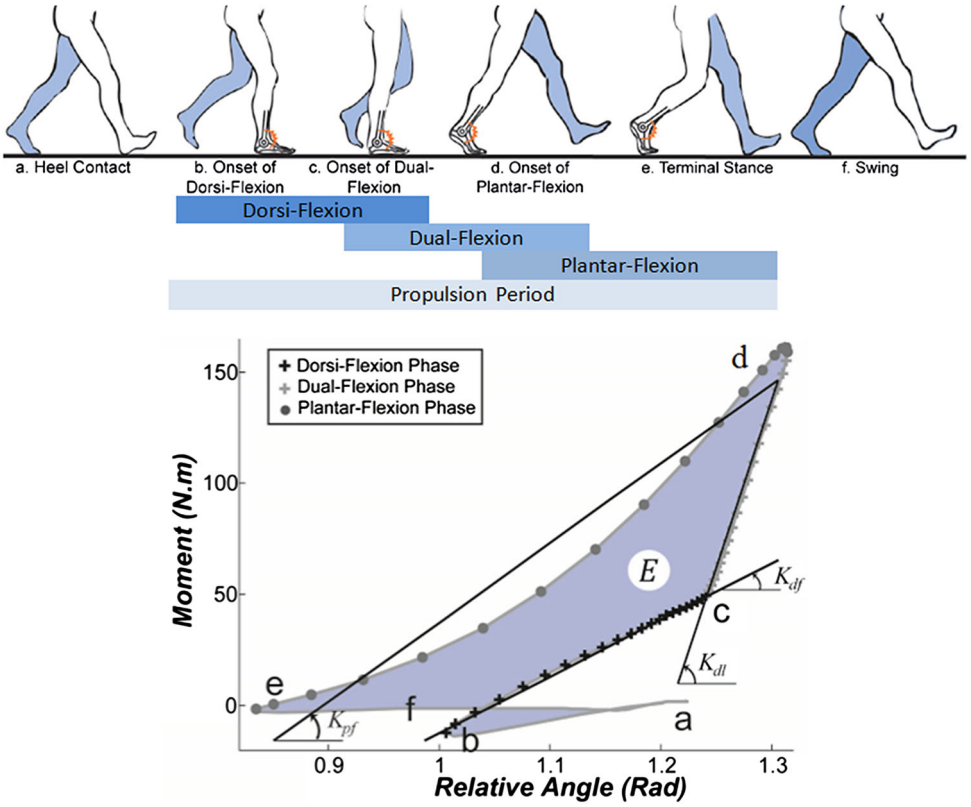

Fig. 1 Human ankle moment versus relative angle curve [31]

characteristics are antagonistically coupled while working against each other with two different motors [8]. The schematic view of the design is shown in Fig. 2. It can be seen that the stiffness and the equilibrium point of the actuator can be adjusted by controlling the position of the nonlinear springs by two different motors.

To calculate the power requirement and the energy consumption for the antagonistic-controlled actuator design, a simple linear antagonistic setup is used. As shown in Fig. 2, x_1 and x_2 are the position of the first and second motors, respectively. Each position can be independently controlled. x_1 and x_2 can be determined from:

$$x_1 = \frac{F_{\text{ank}}}{K_{\text{yank}}} + y_{\text{ank-bio}} + \frac{K_{\text{yank}}}{4 * K} \tag{1}$$

$$x_2 = \frac{F_{\text{ank}}}{K_{\text{yank}}} + y_{\text{ank-bio}} - \frac{K_{\text{yank}}}{4 * K} \tag{2}$$

where F_{ank}, K_{yank} and $y_{\text{ank-bio}}$ are the force output of the ankle, the desired stiffness value and the biomechanics position data of the ankle, respectively. The symbol K is the mechanical quadratic spring constant used in the actuator design ($F_{\text{spring}} = K * x^2$). All details are given in Ref. [6]. The forces of the first motor (F_1) and the second motor (F_2) are given as:

$$F_1 = K * [y_{\text{ank-bio}} - x_1]^2 \tag{3}$$

$$F_2 = K * [x_2 - y_{\text{ank-bio}}]^2 \tag{4}$$

Hence, the power requirement (P) and the energy consumption (W) of a linear antagonistic actuator can be calculated as:

$$P = F_1 * \dot{x}_1 + F_2 * \dot{x}_2 \tag{5}$$

$$W = \int |F_1 * \dot{x}_1| \mathrm{d}t + \int |F_2 * \dot{x}_2| \mathrm{d}t \tag{6}$$

2.2.2 The mechanically controlled actuator design

In the mechanically controlled actuator design, the stiffness of the actuator is adjusted by the mechanical controller [14]. The stiffness adjustment is done by changing the pretension or preload of the springs used in the design. Figure 3 shows the schematic view of the mechanically controlled actuator design. The first motor (M_1) drives the twin ball-screw mechanism with double nuts and provides the movement of the nonlinear springs. Hence, the stiffness of the actuator can be consistently adjusted by the first motor (M_1), while the second motor (M_2) controls the equilibrium point of the actuator.

As shown in Fig. 3, x_1 and x_2 are the position of the first and second motors and given as:

$$x_1 = -\frac{F_{\text{ank}}}{K_{\text{yank}}} + y_{\text{ank-bio}} - \frac{K_{\text{yank}}}{4 * K} \tag{7}$$

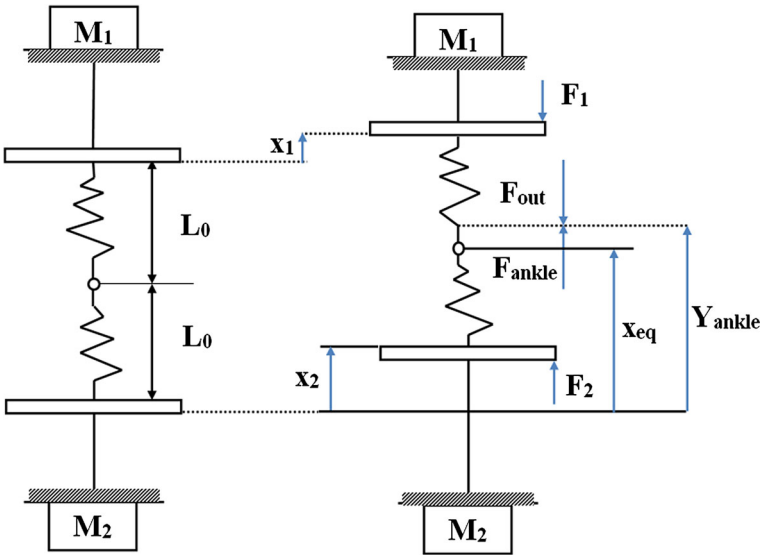

Fig. 2 Schematic view of the antagonistic-controlled actuator design [8]

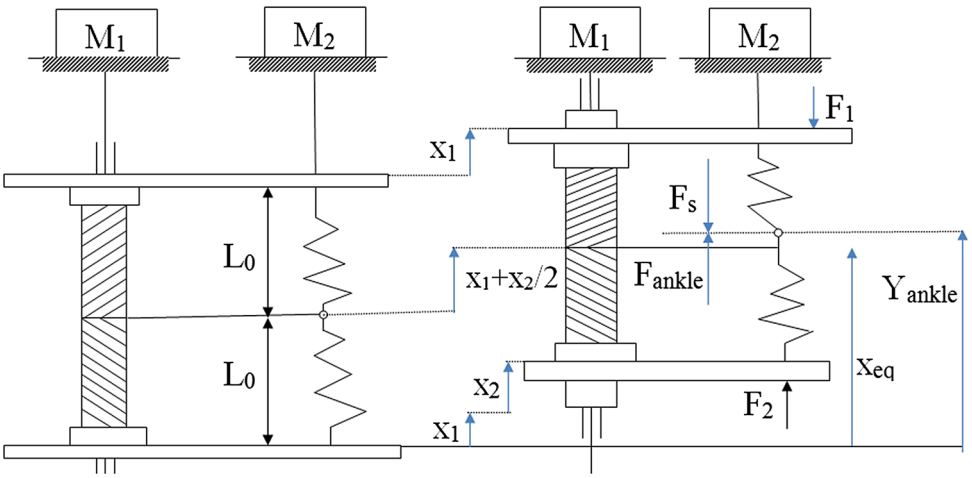

Fig. 3 Schematic view of the mechanically controlled actuator design [14]

$$x_2 = \frac{K_{\text{yank}}}{2 * K} \tag{8}$$

where F_{ank}, K_{yank}, $y_{\text{ank-bio}}$ are force output of the ankle, the desired stiffness value and the biomechanics position data of the ankle, respectively. The symbol K shows the mechanical quadratic spring constant used in the design as it was also used for the same purpose in antagonistic design ($F_{\text{spring}} = K * x^2$). All details are given in Ref. [6]. Equations (9) and (10) are used to calculate the forces of the first motor (F_1) and the second motor (F_2), respectively.

$$F_1 = K * [(x_1 + x_2) - (y_{\text{ank}} - L_o]^2 \tag{9}$$

$$F_2 = K * \left[-\frac{F_{\text{ank}}}{K_{\text{yank}}} + \frac{K_{\text{yank}}}{4 * K} \right]^2 \tag{10}$$

Finally, for the mechanically controlled actuator design, power requirement (P) and energy consumption (W) can be calculated as:

$$P = F_1 * \dot{x}_1 + F_2 * \dot{x}_2 \tag{11}$$

$$W = \int |F_1 * \dot{x}_1| \mathrm{d}t + \int |F_2 * \dot{x}_2| \mathrm{d}t \tag{12}$$

2.2.3 The controllable transmission ratio actuator design

Figure 4 shows the schematic view of our variable stiffness actuator which is based on a changing transmission ratio mechanism via lever. Hence, it is named as the controllable transmission ratio actuator. The compliant actuators in this class change transmission ratio between the spring deflection and the input force through variation of a lever arm mechanism. As shown in Fig. 4, the stiffness of the mechanism is adjusted by changing the transmission ratio between the spring and the force point. The stiffness is adjusted by controlling the position of the lever arm with a second motor, while the pivot and spring points are fixed.

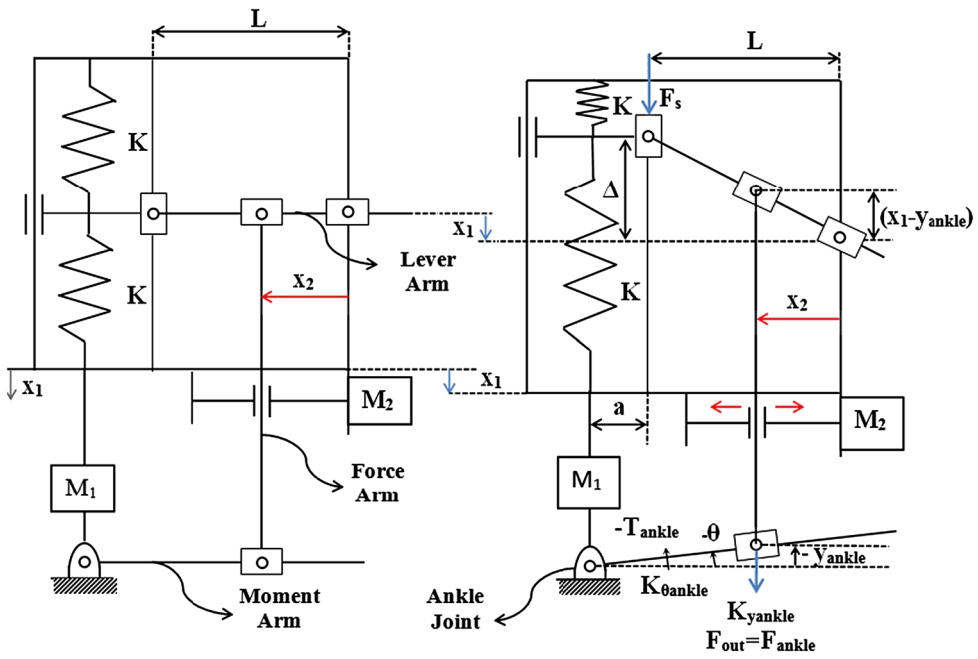

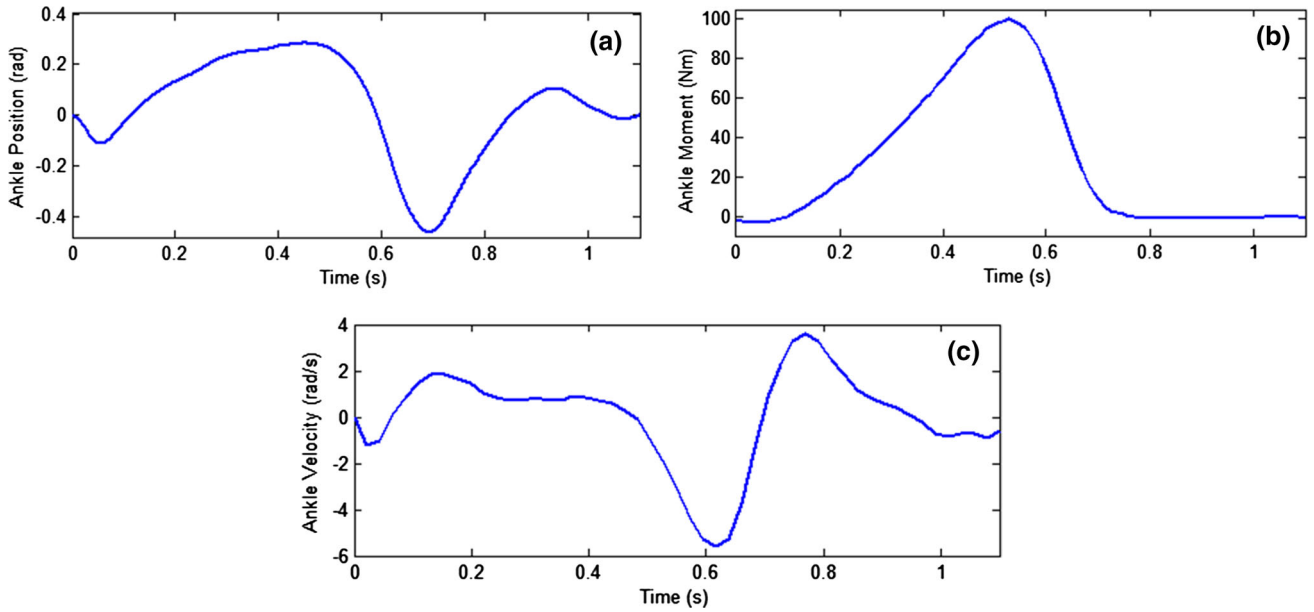

Fig. 4 Schematic view of the controllable transmission ratio actuator

Fig. 5 **a** Angle, **b** moment and **c** velocity of the ankle during gait cycle

The second motor (M_2) performs the stiffness adjustment, while the first motor (M_1) controls the equilibrium point of the whole mechanism.

As shown in Fig. 4, x_1 represents the equilibrium position of the whole mechanism and is controlled by the first motor (M_1). Equation (13) is used to calculate the required position of the first motor for the ankle moment and is given as:

$$x_1 = (a + L - x_2) * \tan(\theta_{\text{ank}}) + \frac{T_{\text{ank}} * x_2^2}{2 * L^2 * (a + L - x_2) * K} \tag{13}$$

where θ_{ank},T_{ank}, K and L are the angle of the ankle, torque of the ankle, mechanical spring constant used in the design and total length of the lever arm, respectively. The variable length of the lever arm x_2 is controlled by the second motor

for the adjustment of the ankle stiffness and is calculated as:

$$x_2 = \frac{(a+L)*L}{l+\cos\theta_{\text{ank}} * \sqrt{\frac{K_{\theta\text{ank}}}{2*K}}} \tag{14}$$

In Eq. (14), $K_{\theta\text{ank}}$ represents the desired stiffness of the ankle. It depends on the mechanical spring constant (K), total length of the lever arm (L), joint angle of the ankle (θ_{ank}) and variable length of the lever arm (x_2). As understood from this equation, the variation of the stiffness is not linear with respect the variable length of the lever arm (x_2) and joint's angle variable (θ_{ank}).

The forces applied by the first and second motors are expressed as:

$$F_{m1} = -2*K*\frac{L^2}{x_2^2}[(a+L-x_2)*\tan\theta_{\text{ank}}] \tag{15}$$

$$F_{m2} = F_{\text{ank}} * [\cos\alpha * \sin\alpha + \cos\theta_{\text{ank}} * \sin\theta_{\text{ank}}] \tag{16}$$

where $\alpha = \arctan\left[\frac{x_1-(a+L-x_2)*\tan\theta_{\text{ank}}}{x_2}\right]$.

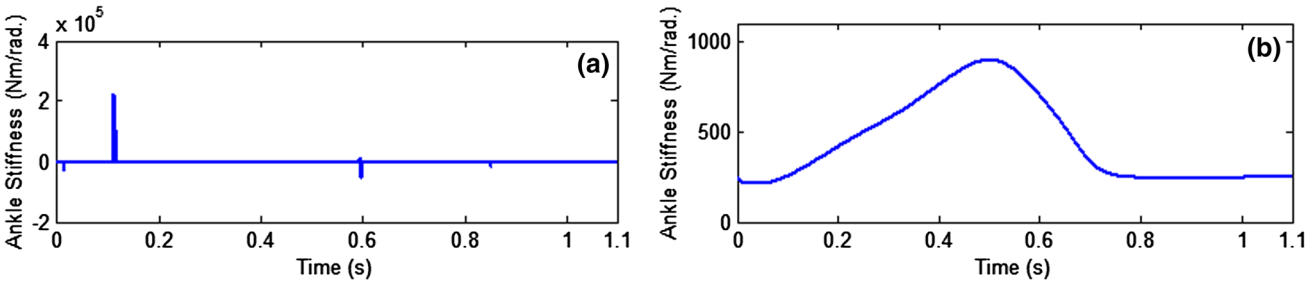

Fig. 6 **a** Calculated stiffness and **b** modified stiffness values

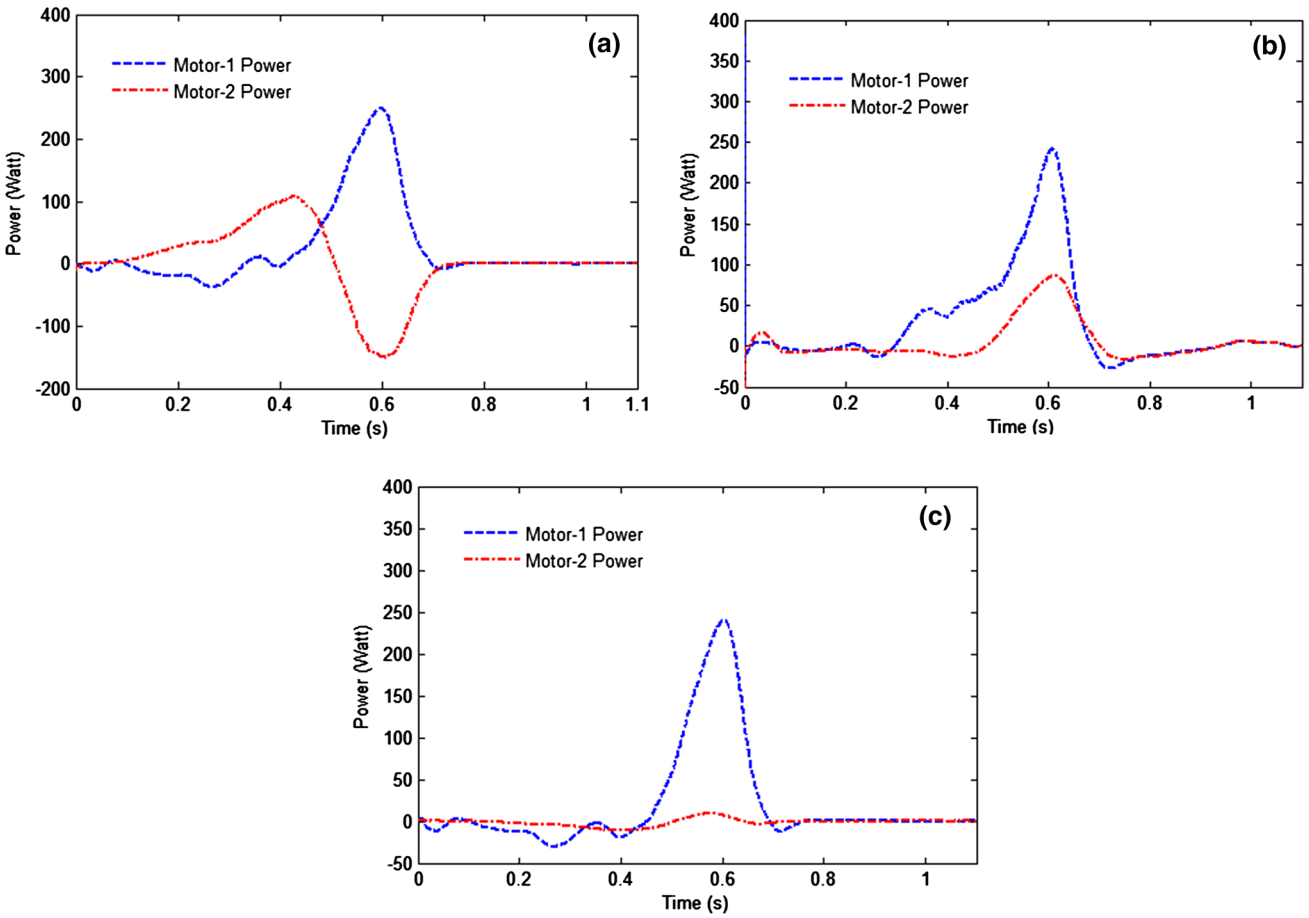

Fig. 7 Power requirement of **a** antagonistic-controlled, **b** mechanically controlled and **c** controllable transmission type actuator designs

Equations (17) and (18) are used to calculate the power requirement (P) and the energy consumption (W):

$$P = P_{m1} + P_{m2} = F_{m1} * \dot{x}_1 + F_{m2} * \dot{x}_2 \quad (17)$$

$$W = \int |F_1 * \dot{x}_1| \mathrm{d}t + \int |F_2 * \dot{x}_2| \mathrm{d}t \quad (18)$$

2.2.4 Comparison of different actuator types

In this section, the simulation results are presented in cases of the antagonistic-controlled, the mechanically controlled and the controllable transmission ratio actuator designs for an ankle joint. The three designs are compared in terms of power requirement and energy consumption. Before starting the simulation studies, biomechanics data like position, velocity and moment of the joint are needed for the ankle joint with which the designs will be tested. Therefore, it is firstly preferred biomechanics data by provided Bovi et al. [33]. The biomechanics data vary depending on weight, height and walking speed of a human. For this reason, it was chosen ankle angle, velocity and moment values of an optimum walking speed ($0.8 \leq$ walking speed/height ≤ 1) of an adult person with 80 kg weight and 170 cm height in the simulations. Angle, velocity and moment plots of the ankle during the gait cycle are shown in Fig. 5.

To calculate the stiffness of ankle during gait cycle, the moment values are divided to the angle values and the results are shown in Fig. 6a. This stiffness variation can be provided by any variable stiffness actuator since it sharply changes. Therefore, the stiffness value should be modified.

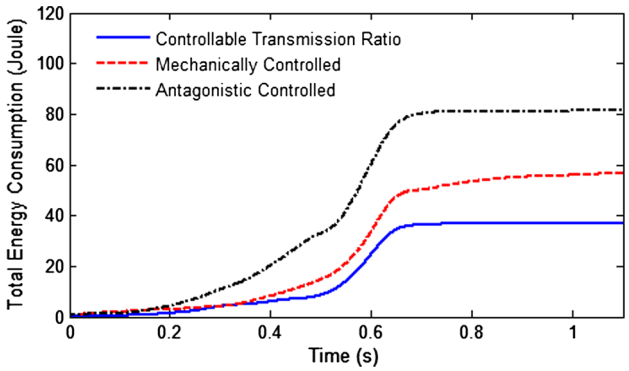

Fig. 9 Total energy consumption for the three designs

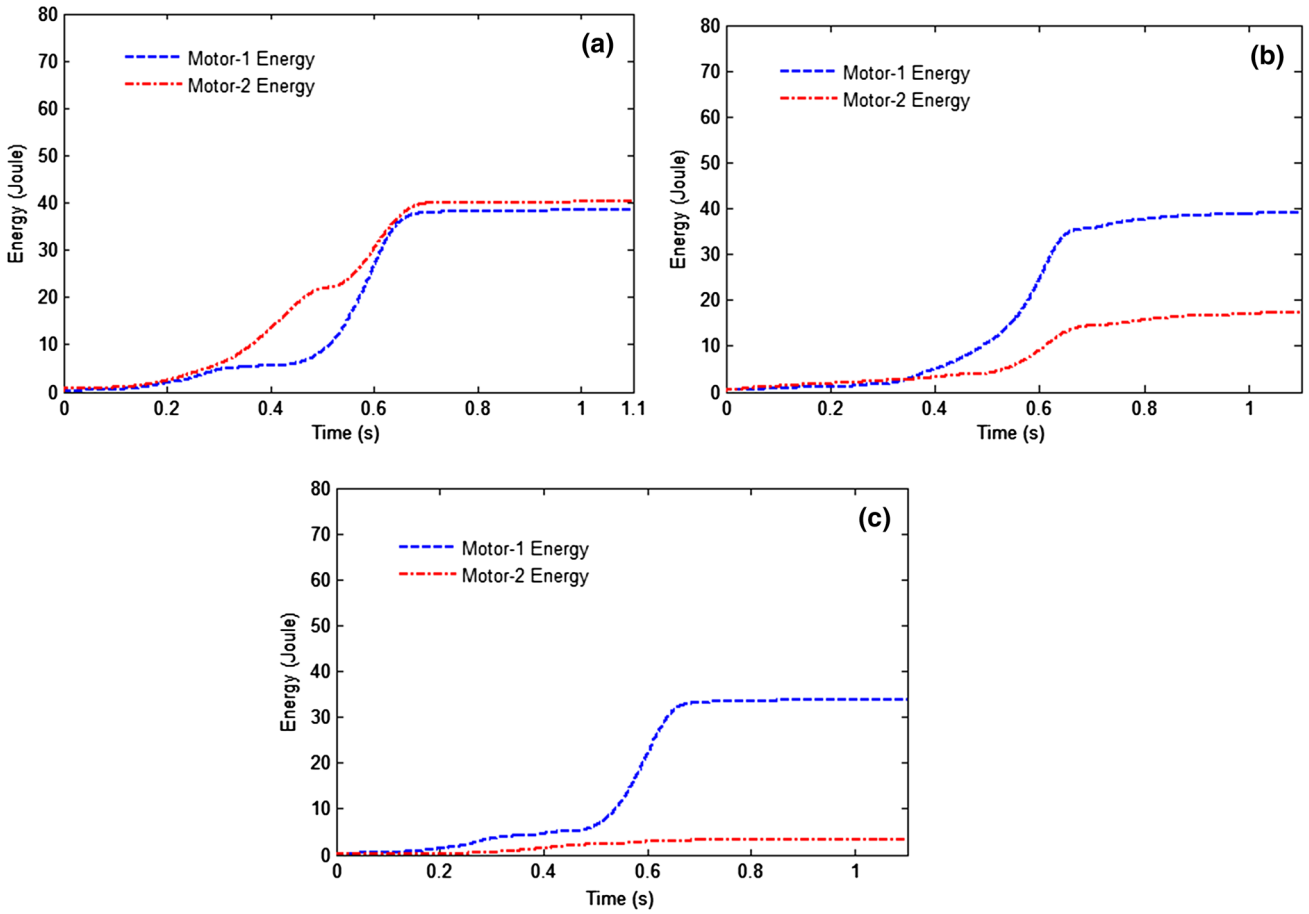

Fig. 8 Energy consumption of **a** antagonistic-controlled, **b** mechanically controlled and **c** controllable transmission type actuator designs

For this reason, a method proposed by Holgate et al. [34] was used and a modified stiffness value was obtained shown in Fig. 6b. All details are given in Ref. [6].

In the simulation studies, the modified stiffness values given in Fig. 6b and angle and torque values of the ankle given in Fig. 5 are taken as reference values. The simulation tests for three different actuator designs were carried out by using the equations obtained in the previous sections of the actuator designs. As a result of the simulations, the power requirement of motors in each design is given in Fig. 7. As seen in Fig. 7, while the first motors in the designs need 250 W, the second motors have quite different power needs. According to the reference simulation scenario, while the second motors in the antagonistic and mechanically controlled actuator designs need 100 W power requirement, the second motor in the controllable transmission ratio actuator design needs 10 W. Therefore, it is possible to work with smaller motors in the controllable transmission ratio actuator design. Figure 7 also shows that the ankle is strongly loaded in the propelling the body forward within the last of stance phase (45–60% of the gait cycle that is the half way of gait cycle time). Therefore, the power of the motors in the designs increases considerably at the end of the stance phase (45–60% of the gait cycle) and then decreases at the swing phase.

The energy consumption of the motors can be calculated by the area under power plots. Figure 8 shows the consumed energy of the motors in the designs. As seen in Fig. 8, even though the first motors in the designs have similar energy consumption, there are significant differences in the energy consumption of the second motors. The second motors consume 40 Joule energy in the antagonistic-controlled, 15 Joule energy in the mechanically controlled and 3 Joule energy in the controllable transmission ratio actuator designs.

The stiffness and equilibrium position can be controlled independently in the controllable transmission ratio actuators, while they can be set by controlling both motors at the same time in the antagonistic-controlled and the mechanically controlled actuators. Hence, the controllable transmission ratio actuator requires less power and energy consumption compared to the other actuator designs. Lastly, the total energy consumed by motors is given for three designs. Figure 9 shows energy consumptions in the antagonistic-controlled (80 J), actuator mechanically controlled actuator (55 J) and the controllable transmission ratio actuator (37 J) during a gait cycle. The energy

Table 1 General specifications of VS-AnkleExo

Range of motion	30° (Dorsi-flexion)
	50° (Plantar-flexion)
Time to change the stiffness (s)	3.06
Height (mm)	420–460
Width (mm)	70
Weight (kg)	3
Maximum payload (Nm)	100

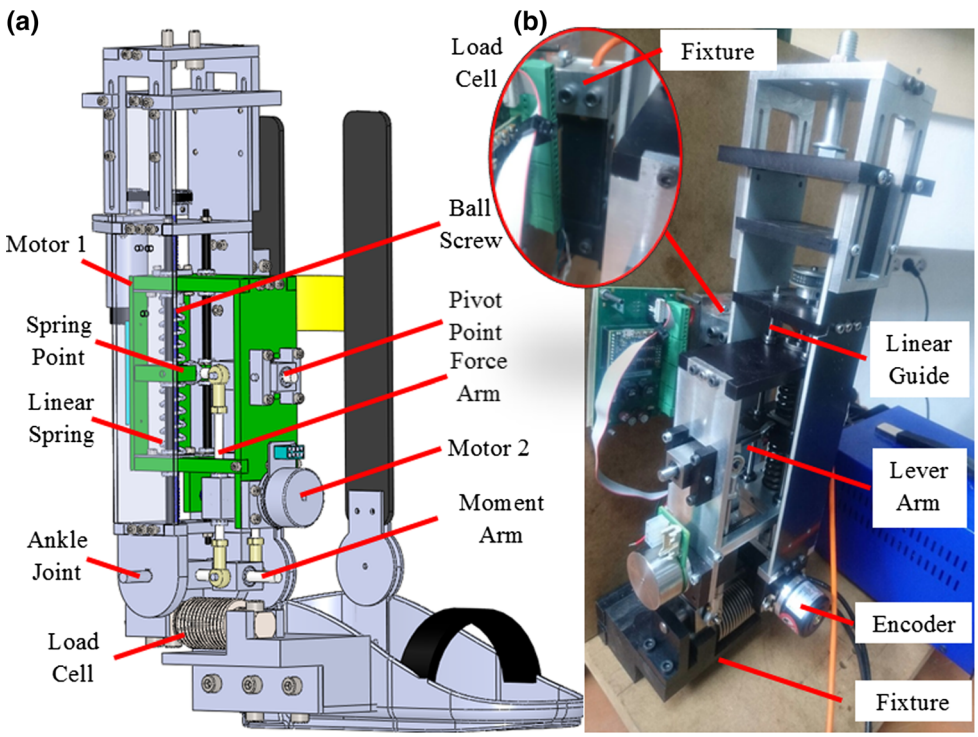

Fig. 10 **a** CAD design of VS-AnkleExo while output link is unloaded and **b** the actuator is at the highest stiffness

consumption difference between the controllable transmission ratio actuator and the other two designs is important for mobile human-like robots operated on batteries. As a result, the controllable transmission ratio actuator proposed in this study is more feasible than the other actuator types for the exoskeleton of the ankle joint.

2.3 Mechanical design of VS-AnkleExo

VS-AnkleExo is designed as an ankle exoskeleton with a variable stiffness actuator for rehabilitation and power augmentation purposes. The design to adjust the stiffness is based on the controllable transmission ratio mechanism. In this mechanism, a lever rotates around a pivot point, while two springs antagonistically attached are fixed and the load point varies on the lever. The length of the lever arm is defined as a distance between the pivot and load points. Hence, the stiffness of the mechanism can be adjusted by changing the length of the lever arm.

Figure 10 shows the design of VS-AnkleExo. The design involves a variable stiffness actuator, embedded force sensors, a lower limb adjustment mechanism and an ankle foot orthosis. Motor 1 (Brushless Direct Current Motor (BLDC), 200 W, EC-4pole 30, Maxon Motor AG, Switzerland) is used to provide a continuous torque for the joint which moves up and down a box-shaped mechanism with a ball screw. Hence, the position of the ankle joint is changed with the force arm on the lever and the moment arm. To obtain the variable stiffness, a linear motion

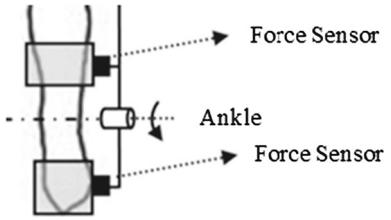

Fig. 12 Placement of the force sensors

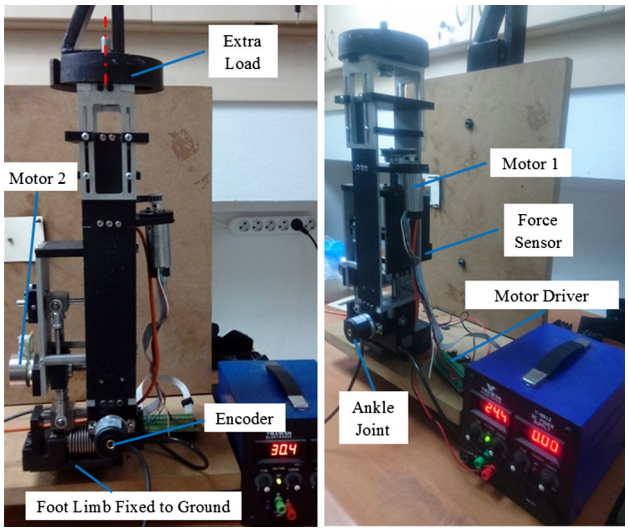

Fig. 13 Experimental setup used for the transparency experiments

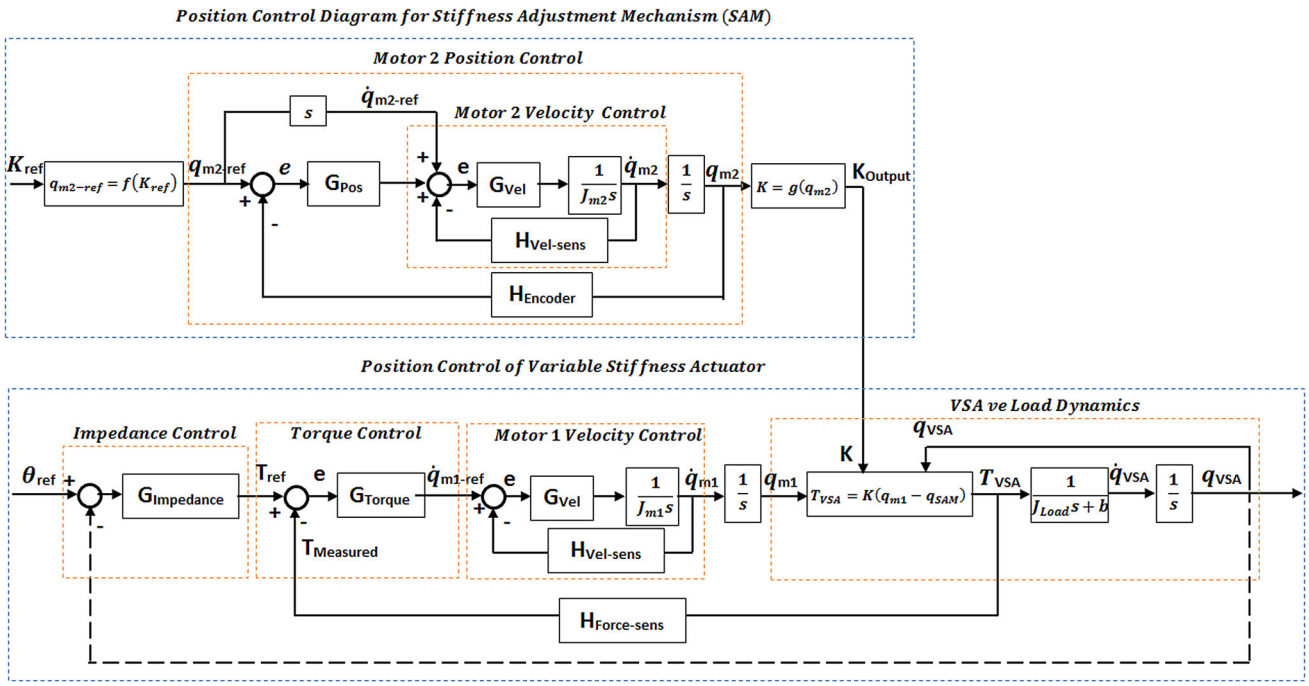

Fig. 11 The impedance control of the variable stiffness actuator and position control diagram for stiffness adjustment mechanism

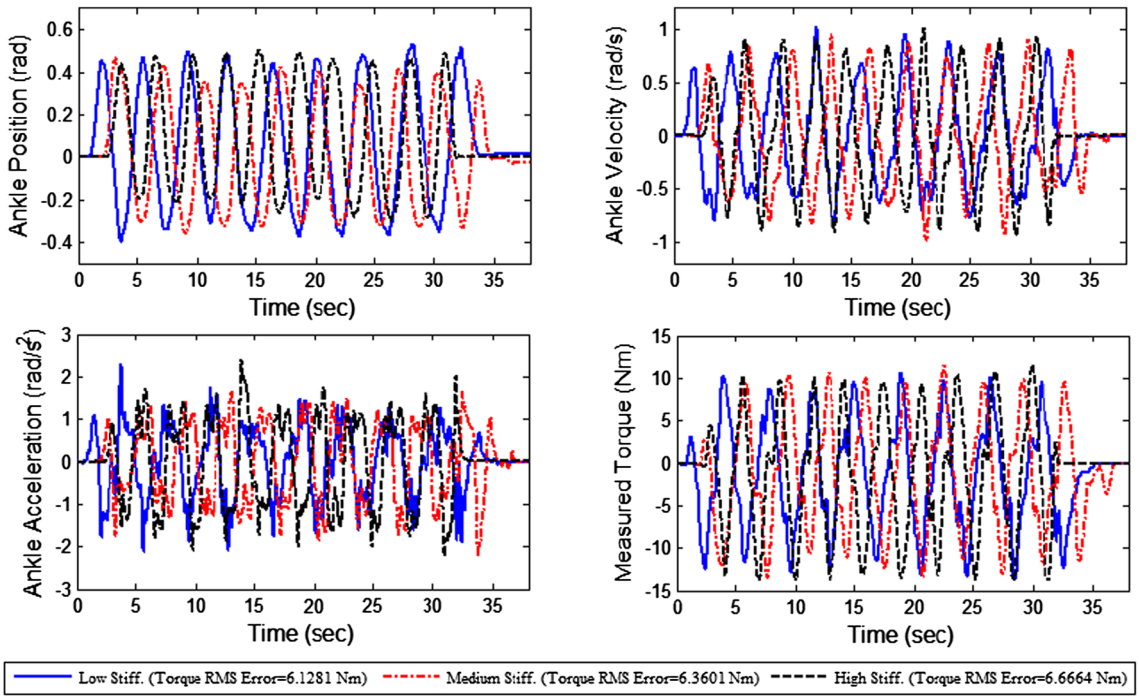

Fig. 14 No-control transparency performance experiment with low (full line), medium (dash-dot line), high (dash line) stiffness and torque RMS errors

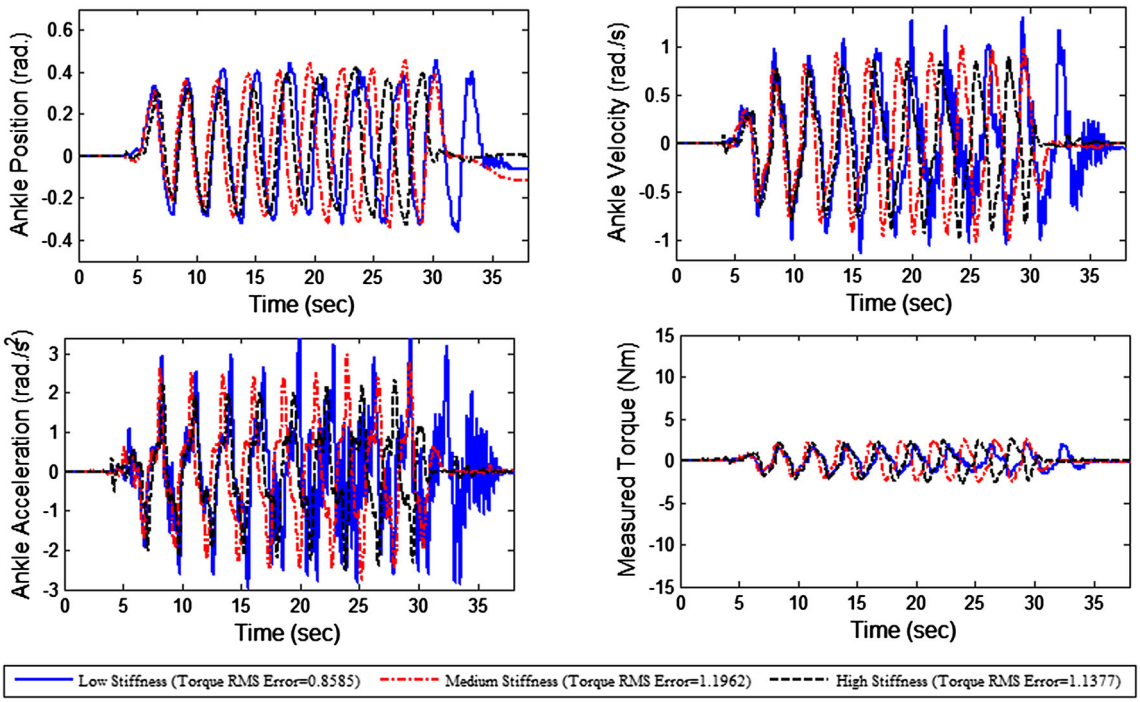

Fig. 15 Impedance-control transparency performance experiment with low (full line), medium (dash-dot line), high (dash line) stiffness and torque RMS errors

mechanism is designed (Fig. 10). In this mechanism, Motor 2 (BLDC, 70 W, EC45 flat, Maxon Motor AG, Switzerland) is directly connected to ball screw to control the position of the force arm on the lever with a rolling the ball screw. Thus, stiffness adjustment of the actuator is achieved on the actuator. In this design, four types of

materials were used: kestamid, aluminum, steel and composite sheets. The stiffer ones were used for critical regions like joint shafts, joint bearings and lever arms, while the lights were used for the others. There are better materials with high strength and low density, like more expensive titanium alloys. However, these materials were selected due to the low cost and availability.

In wearable robotic devices, the interaction forces are important for comfort and safety. Hence, two force sensors are employed in the design to measure the interaction forces. The first sensor is used to measure the ground reaction forces during the contact of robotic device with the ground. The other force sensor measures the interaction forces between the shank of the user and robotic device. Another part of VS-AnkleExo is a lower limb adjustment mechanism. This mechanism is designed to adapt VS-AnkleExo for users with different shank length. An ankle foot orthosis is used to transfer the motion of the device to the user. The general specifications of VS-AnkleExo are provided in Table 1. One may consider that this design is large and heavy. In this respect, it should be noted that VS-AnkleExo design presented in this paper is the shank part of a complete lower limb exoskeleton. It is not for a stand-alone active ankle orthosis. It will be incorporated into a complete lower extremity exoskeleton. VS-AnkleExo includes not only actuation mechanisms but also shank segment parts of the complete lower limb exoskeleton.

2.4 Controller design

An impedance control diagram is developed to control VS-AnkleExo. Figure 11 shows the block diagram of the force/torque feedback control method developed for this purpose. The control algorithm developed is used to increase the interactions between the robot and the user, and to ensure that VS-AnkleExo can track the input torque profile. The control diagram developed has multiple segments as shown in Fig. 11. The inner velocity control loop uses G_{Velocity}, while G_{Torque} controller is used for the outer torque control loop. In addition to these controllers, the outer impedance controller incorporates a $G_{\text{Impedance}}$ controller. Moreover, the load dynamics are defined with inertia and damping constant. The impedance controller generates a reference torque (T_{ref}) based on the impedance required ($G_{\text{Impedance}}$) around the equilibrium position (θ_{ref}). Based on VS-AnkleExo actuator design, the feedback signal generated by the actuator can be determined from the following expression:

$$T_{\text{VSA}} = K * (q_{m1} - q_{\text{VSA}}) \tag{19}$$

Moreover, the torque controller generates a reference signal ($\dot{q}_{m1-\text{ref}}$) for the velocity controller. To determine the performance of the controller and the designed device, transparency experiments are carried out. In these experiments, the goal is to minimize the residual forces on the user when the user interacts with the device. Since the aim of the experiments is to reduce the forces as much as possible, the value for $G_{\text{Impedance}}$ is taken as zero during the transparency experiments. Moreover, a second motor is used to control the actuator stiffness. To control this motor, a second position control loop is implemented as shown in Fig. 11. Hence, the transparency experiments are carried out in two configurations: (1) constant stiffness and (2) variable stiffness. $G_{\text{Impedance}}$ is not zero for other impedance control applications except for the transparency. Therefore, in addition to the transparency experiments, the device ability to track a reference torque signal is characterized with tracking performance experiments.

3 Results and discussion

3.1 Transparency experiments

The transparency experiments were carried out to determine whether the controller could minimize the forces between the user and robotic system developed. To measure the interaction forces, force sensors were attached to the locations where the user interacts with the robot as shown in Fig. 12. In these experiments, the robot was used in "human-in-charge" mode while aiming to minimize the forces measured by the force sensors.

The details of experimental test setup used for VS-AnkleExo during the transparency experiments are shown in Fig. 13. For the transparency experiments, the foot part of the robot was fixed on the ground, while the leg was not constrained to obtain free movement. Moreover, a 50 N additional load was added to the device to show the performance of the controller implemented. The experiments were carried out for three different stiffness values designated as low, medium and high. The experiments were repeated for the cases where the controller was active and inactive.

Figure 14 shows the ankle position, velocity, acceleration and the measured torques from the sensors for different constant stiffness values without the control system being active. In these experiments, the variable ankle angle was provided as an input to the device by the user, while ankle velocity and acceleration, and measured torque were obtained from the system. Figure 15 shows the experimental results obtained for different constant stiffness where the control system was active.

It should be noted that the ankle position input to the device was provided manually by the user while aiming to obtain similar velocity and acceleration profiles. The results of the transparency experiments with constant

actuator stiffness show the device exerts a varying torque with a maximum value of 10 Nm to the user when the controller is not active. On the other hand, the torque values measured from the torque sensors were significantly reduced when the controller was active. These results show that the designed controller diagram for VS-AnkleExo can reduce the residual torques exerted on the user when the actuator stiffness is constant.

The previous experiments were carried out at constant stiffness values. To determine the performance of the control system under varying stiffness based on the ankle angle, additional experiments were carried out where the stiffness was varied. A linear function was defined to relate the ankle stiffness as a function of the ankle angle for the experiments. Note that this function is not stiffness variation of a gait cycle; it is only a sample stiffness variation to test the controller for the transparency of the device under varying stiffness.

$$K_{\text{ankle}}(\theta_{\text{ankle}}) = K_{\text{starting}} - A * [\theta_{\text{ankle}}] \tag{20}$$

where K_{angle}, K_{starting} and A are ankle stiffness, initial ankle stiffness and a constant, respectively. This experiment was carried out with human ankle joint. Integration of VS-AnkleExo to human ankle joint is shown in Fig. 16. Figure 17 shows the results of the transparency experiments with varying ankle stiffness as a function of ankle angle.

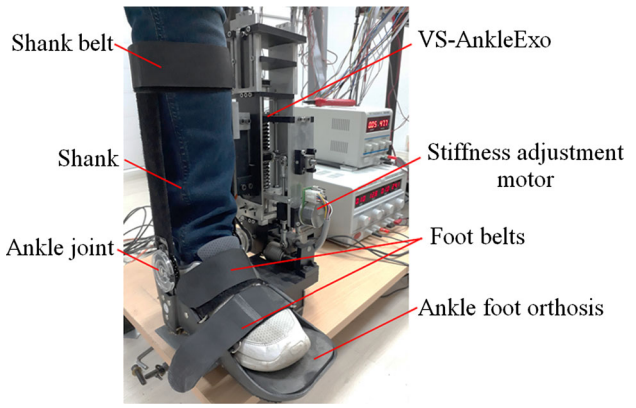

Fig. 16 Integration of VS-AnkleExo to human ankle joint

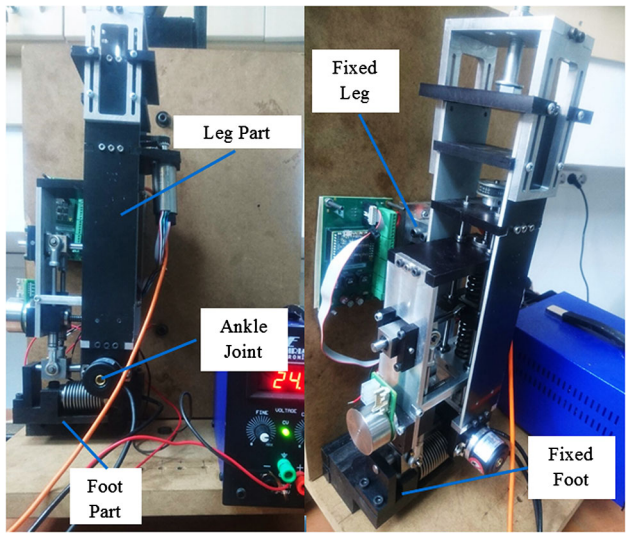

Fig. 18 Experimental setup for tracking performance

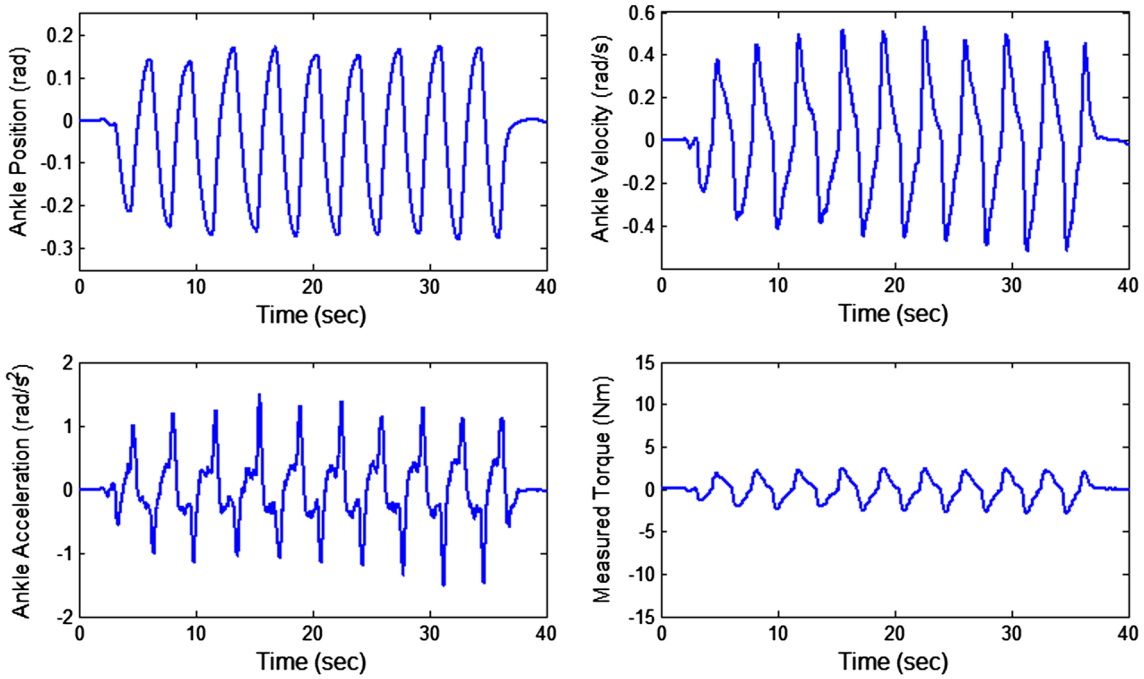

Fig. 17 Impedance-control transparency performance experiment with variable stiffness

The controller was able to reduce the forces exerted on the user by the device, allowing users to carry out certain tasks without experiencing the resistance of the device.

3.2 Tracking performance experiments

In addition to the transparency experiments, the device performance was also characterized by carrying out tracking performance experiments. In these experiments, the goal was to determine whether the system coupled with the impedance control algorithm can track the input torque profile. To carry out these experiments, a test setup shown in Fig. 18 was used. In these experiments, both the foot and leg parts of the robot were constrained to a platform. Sinusoidal torque profiles with different frequencies were provided to the system, and the tracking ability of the device was determined by comparing the input signals to the torque generated by the system. The results of the experiments are shown in Fig. 19.

The control system implemented for VS-AnkleExo was able to track the input torque profile for various stiffness at different frequencies. It should be noted that a phase shift between the input and the output signals was observed during the experiments as the frequency of the input signals increased. These phase shifts were reduced when the stiffness of the actuator was low. Moreover, the same PID parameters were used for all of the experiments without tuning the PID parameters for each individual experiment.

To measure the closed-loop torque control bandwidth of VS-AnkleExo, a white noise torque reference with 100 Nm amplitude for 10 s was used as a controller reference signal and output torque was recorded. Then, a transfer function was estimated as a function of frequency by dividing the cross-power spectral density between the torque input and torque output by the power spectral density of the torque input. Same experiments were repeated for low, middle and high stiffness cases of VS-AnkleExo. Figure 20 shows that the closed torque control bandwidths of VS-AnkleExo (7 Hz, 10 Hz and 12 Hz for low, middle and high device stiffness, respectively).

Finally, in order to find the time response of VS-AnkleExo, the test setup in Fig. 18 was again used such that both the foot and leg parts of the actuator were fixed to a platform. A step input reference of 1 Nm was applied to the system; this experiment was repeated for three stiffness values: low, medium and high. Figure 21 shows the time response results of the system for this constant torque input. VS-AnkleExo presents 4% overshoot and 0.07 s settling time for low stiffness, 9% overshoot and 0.06 s settling time for medium stiffness and %14 overshoot and 0.05 s settling time for high stiffness, which are very fast. These parameters are compatible with the reference works results [35, 36].

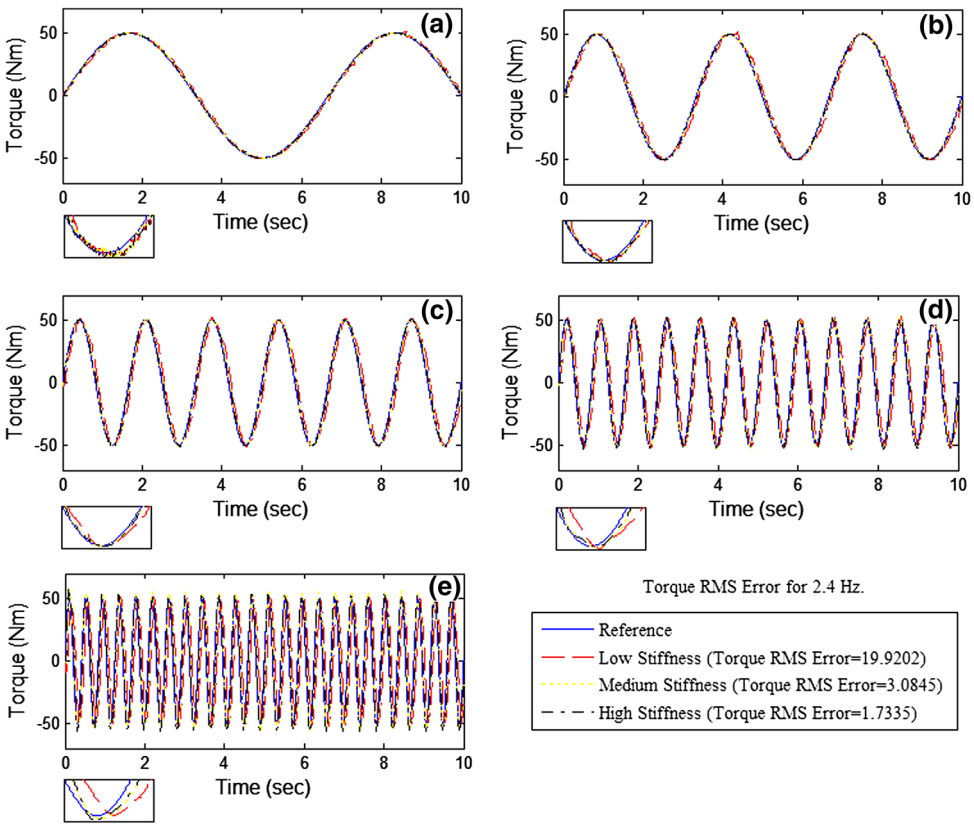

Fig. 19 Closed-loop force/torque control diagram experiment with low, medium and high stiffness, **a** $f = 0.15$ Hz, **b** $f = 0.3$ Hz, **c** $f = 0.6$ Hz, **d** $f = 1.2$ Hz, **e** $f = 2.4$ Hz

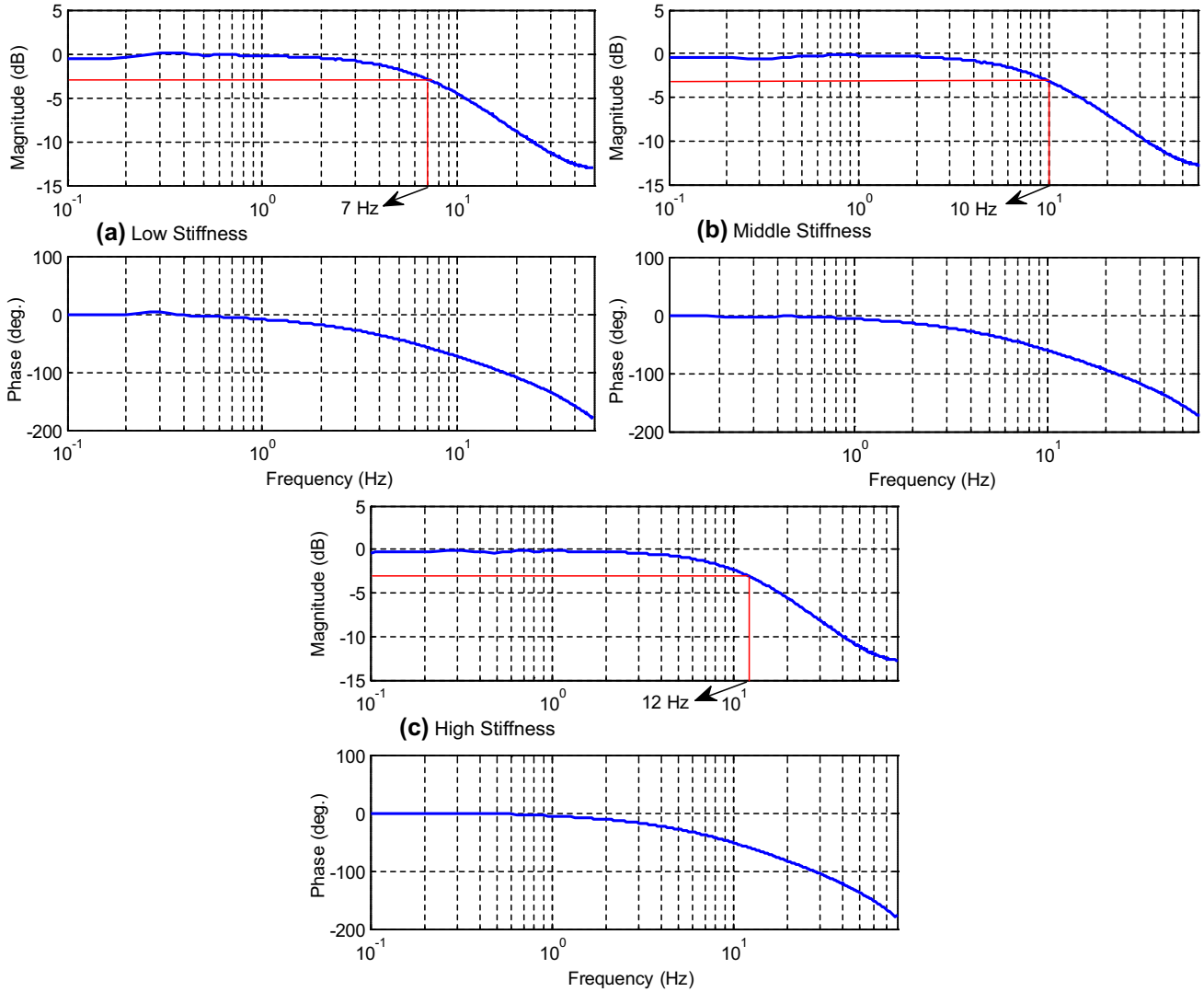

Fig. 20 Bode diagrams of the closed-loop torque control for **a** high, **b** middle and **c** high stiffness of VS-AnkleExo

4 Conclusions and future works

This research presents a new compliant actuator with adjustable stiffness intended for a lower limb wearable ankle robot called VS-AnkleExo. The developed actuator is capable of adjusting the stiffness through a controllable transmission ratio mechanism. The system developed was compared to the other actuator types such as the antagonistically controlled and mechanically controlled actuators. It was shown that the new actuator design presented in this work has less power requirement and energy consumption compared to the available actuator designs. Moreover, it was shown that the required energy to change the stiffness of the actuator is minimal when the output link of the system is not loaded in the actuator.

An impedance controller was designed and implemented to control VS-AnkleExo. The performance of the control system was experimentally characterized through transparency and tracking performance experiments. Transparency experiments were carried out to show that the forces between user and robot in human-in-charge mode were reduced at various stiffness values. The experimental results showed that the control system was able to significantly reduce the forces measured during the transparency experiment. Moreover, the device's torque tracking ability was characterized with tracking performance experiments where sinusoidal torque inputs with different frequencies were provided. Then, the device's tracking performance was determined by comparing the input and output torque signals. The experimental results showed that the actuator designed is able to track the given input torque signal at various frequencies fairly well. The future work aims to implement a new control diagram for the system allowing simultaneous position and stiffness tracking control.

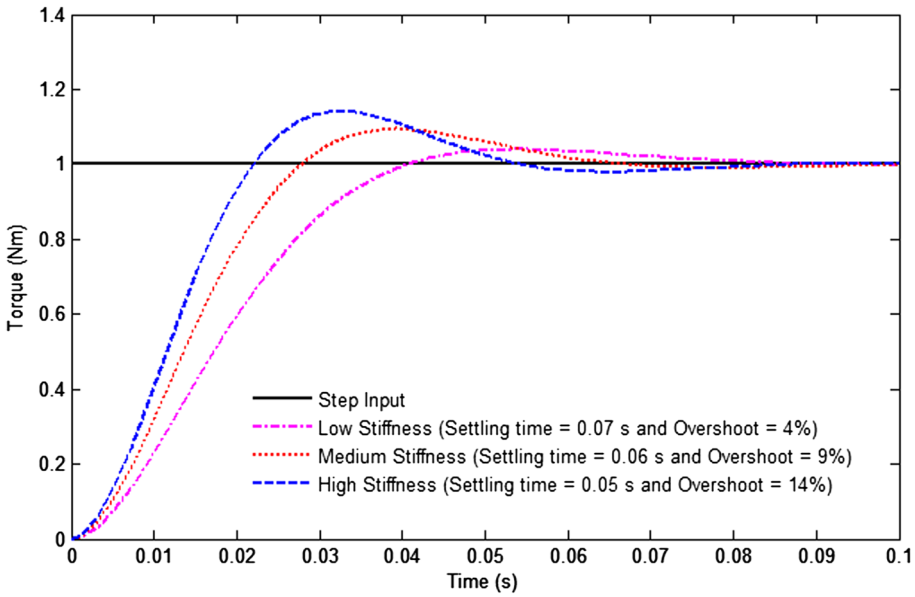

Fig. 21 Time response of VS-AnkleExo for **a** low, **b** medium and **c** high stiffness values

Moreover, the design of VS-AnkleExo will be improved and incorporated into a complete lower limb exoskeleton robot.

Acknowledgements The author would like thank to TUBITAK (The Scientific and Technological Research Council of Turkey) for the financial support of a research Project Numbered with 213M297, and Ozan Erol and Ergin Kilic for their inputs for manuscript preparation.

References

1. Banala S, Agrawal K, Fattah SK, Krishnamoorthy V, Hsu WL, Scholz J, Rudolph K (2016) Gravity-balancing leg orthosis and its performance evaluation. IEEE Trans Rob 22(6):1228–1239
2. Agrawal SK, Banala SK, Fattah A, Sangwan V, Krishnamoorthy V, Scholz JP, Hsu WL (2007) Assessment of motion of swing leg and gait rehabilitation with a gravity balancing exoskeleton. IEEE Trans Neural Syst Rehabil Eng 15(3):410–420
3. Rahman T, Sample W, Seliktar R (2004) Design and testing of wrex. In: Bien ZZ, Stefanov D (eds) Advances in rehabilitation robotics, vol 306. Springer, Berlin, Heidelberg, pp 243–250
4. De Santis A, Siciliano B, De Luca A, Bicchi A (2008) An atlas of physical human–robot interaction. Mech Mach Theory 43(3):253–270
5. Pratt GA, Williamson MM (1995) Series elastic actuators. In: Proceedings IEEE/RSJ international conference on intelligent robots and systems 95 human robot interaction and cooperative robots 1995, vol 1, pp 399–406
6. Kizilhan H, Baser O, Kilic E, Ulusoy N (2015) Comparison of controllable transmission ratio type variable stiffness actuator with antagonistic and pre-tension type actuators for the joints exoskeleton robots. In: 2015 12th international conference on informatics in control, automation and robotics (ICINCO), vol 2, pp 188–195
7. Tonietti G, Schiavi R, Bicchi A (2005) Design and control of a variable stiffness actuator for safe and fast physical human/robot interaction. In: Proceedings of the 2005 IEEE international conference on robotics and automation, pp 526–531
8. Hurst JW, Chestnutt JE, Rizzi AA (2010) The actuator with mechanically adjustable series compliance. IEEE Trans Rob 26(4):597–606
9. Verrelst B, van Ham R, Vanderborght B, Daerden F, Lefeber D, Vermeulen J (2005) The pneumatic biped "Lucy" actuated with pleated pneumatic artificial muscles. Auton Rob 18(2):201–213
10. Schiavi R, Grioli G, Sen S, Bicchi A (2008) VSA-II: a novel prototype of variable stiffness actuator for safe and performing robots interacting with humans. In: IEEE international conference on robotics and automation, pp 2171–2176
11. Catalano MG, Grioli G, Garabini M, Bonomo F, Mancini M, Tsagarakis N, Bicchi A (2011) Vsa-cubebot: a modular variable stiffness platform for multiple degrees of freedom robots. In: 2011 IEEE international conference on robotics and automation (ICRA), pp 5090–5095
12. Hollander KW, Sugar TG, Herring DE (2005) Adjustable robotic tendon using a'Jack Spring'/spl trade. In: IEEE 9th international conference on rehabilitation robotics, icorr 2005, pp 113–118
13. van Ham R, Vanderborght B, van Damme M, Verrelst B, Lefeber D (2007) MACCEPA, the mechanically adjustable compliance and controllable equilibrium position actuator: design and implementation in a biped robot. Rob Auton Syst 55(10):761–768
14. Wolf S, Hirzinger G (2008) A new variable stiffness design: matching requirements of the next robot generation. In: IEEE international conference on robotics and automation, ICRA 2008, pp 1741–1746
15. Jafari A, Tsagarakis NG, Vanderborght B, Caldwell DG (2010) A novel actuator with adjustable stiffness (AwAS). In: 2010 IEEE/RSJ international conference on intelligent robots and systems (IROS), pp 4201–4206
16. Jafari A, Tsagarakis NG, Caldwell DG (2011) AwAS-II: a new actuator with adjustable stiffness based on the novel principle of adaptable pivot point and variable lever ratio. In: 2011 IEEE international conference on robotics and automation (ICRA), pp 4638–4643
17. Groothuis SS, Rusticelli G, Zucchelli A, Stramigioli S, Carloni R (2012) The vsaUT-II: a novel rotational variable stiffness actuator. In: 2012 IEEE international conference on robotics and automation (ICRA), pp 3355–3360
18. Pratt JE, Krupp BT, Morse CJ, Collins SH (2004) The RoboKnee: an exoskeleton for enhancing strength and endurance during

walking. In: 2004 IEEE international conference on robotics and automation, proceedings. ICRA'04, vol 3, pp 2430–2435
19. Kwa HK, Noorden JH, Missel M, Craig T, Pratt JE, Neuhaus PD (2009) Development of the IHMC mobility assist exoskeleton. In: IEEE international conference on robotics and automation, ICRA'09, pp 2556–2562
20. Vallery H, Veneman J, van Asseldonk E, Ekkelenkamp R, Buss M, van der Kooij H (2008) Compliant actuation of rehabilitation robots. IEEE Rob Autom Mag 15(3):60–69
21. Veneman JF, Ekkelenkamp R, Kruidhof R, van der Helm FC, van der Kooij H (2006) A series elastic-and bowden-cable-based actuation system for use as torque actuator in exoskeleton-type robots. Int J Rob Res 25(3):261–281
22. Cherelle P, Grosu V, Beyl P, Mathys A, van Ham R, van Damme M, Lefeber D (2010) The MACCEPA actuation system as torque actuator in the gait rehabilitation robot ALTACRO. In: 3rd IEEE RAS and EMBS international conference on biomedical robotics and biomechatronics (BioRob), pp 27–32
23. Beyl P, van Damme M, van Ham R, Vanderborght B, Lefeber D (2014) Pleated pneumatic artificial muscle-based actuator system as a torque source for compliant lower limb exoskeletons. IEEE/ASME Trans Mechatron 19(3):1046–1056
24. Cestari M, Sanz-Merodio D, Arevalo JC, Garcia E (2015) An adjustable compliant joint for lower-limb exoskeletons. IEEE/ASME Trans Mechatron 20(2):889–898
25. Hutter M, Remy CD, Hoepflinger MA, Siegwart R (2013) Efficient and versatile locomotion with highly compliant legs. IEEE/ASME Trans Mechatron 18(2):449–458
26. Mosadeghzad M, Medrano-Cerda GA, Saglia JA, Tsagarakis NG, Caldwell DG (2012) Comparison of various active impedance control approaches, modeling, implementation, passivity, stability and trade-offs. In: IEEE/ASME international conference on advanced intelligent mechatronics (AIM), pp 342–348
27. Wang S, Meijneke C, van der Kooij H (2013) Modeling, design, and optimization of Mindwalker series elastic joint. In: 2013 IEEE international conference on rehabilitation robotics (ICORR), pp 1–8
28. Accoto D, Carpino G, Sergi F, Tagliamonte NL, Zollo L, Guglielmelli E (2013) Design and characterization of a novel high-power series elastic actuator for a lower limb robotic orthosis. Int J Adv Rob Syst 10(10):359
29. Liu L, Leonhardt S, Misgeld BJ (2016) Design and control of a mechanical rotary variable impedance actuator. Mechatronics 39:226–236
30. Adams RJ, Hannaford B (2002) Control law design for haptic interfaces to virtual reality. IEEE Trans Control Syst Technol 10(1):3–13
31. Shamaei K, Sawicki GS, Dollar AM (2013) Estimation of quasi-stiffness and propulsive work of the human ankle in the stance phase of walking. PLoS ONE 8(3):e59935
32. Vanderborght B, Albu-Schäffer A, Bicchi A, Burdet E, Caldwell DG, Carloni R, Catalona M, Ganesh G, Garabini M, Grioli G, Haddadin S, Jafari A, Laffranchi M, Lefeder D, Petit F, Stramigioli S, Grebenstein A, Tsagarakis N, van Damme M, van Ham R, Visse L, Wolf S (2013) Variable impedance actuators: a review. Rob Auton Syst 61(12):1601–1614
33. Bovi G, Rabuffetti M, Mazzoleni P, Ferrarin M (2011) A multiple-task gait analysis approach: kinematic, kinetic and EMG reference data for healthy young and adult subjects. Gait Posture 33(1):6–13
34. Holgate MA, Hitt JK, Bellman RD, Sugar TG, Hollander KW (2008) The SPARK (Spring Ankle with Regenerative kinetics) project: choosing a DC motor based actuation method. In: 2nd IEEE RAS & EMBS international conference on biomedical robotics and biomechatronics, pp 163–168
35. Paine N, Oh S, Sentis L (2014) Design and control considerations for high-performance series elastic actuators. IEEE/ASME Trans Mechatron 19(3):1080–1091
36. Robinson D. (2000) Design and analysis of series elasticity in closed-loop actuator force control", PhD. Thesis, Massachusetts Institute of Technology